JOURNAL OF SCIENCE AND EDUCATION, VOLUME 66, ISSUE 2 (2026) 80-87

TẠP CHÍ KHOA HỌC VÀ GIÁO DỤC
ISSN: 1859-1612
Journal homepage: https://tckhgd.dhsphue.edu.vn

Numerical simulation of dispersion properties in CCl_4-infiltrated square photonic crystal fibers

Siu Lol[1], Nguyen Thi Thuy[2], Hoang Trong Duc[2]

[1]Nguyen Du no. 2 High School, Uar Commune, Gia Lai Province

[2]University of Education, Hue University

ARTICLE INFO

Article history:
Received: 27 April 2024
Received in revised form: 21 June 2024
Accepted: 24 June 2024
Published: 20 April 2026

Keywords:
Photonic crystal fibers;
Carbon tetrachloride;
Ultraflat all-normal dispersion;
Supercontinuum generation.

ABSTRACT

The lattice defects, including differences in air hole size and distance between air holes, have contributed significantly to optimizing the dispersion properties of square lattice photonic crystal fibers with the infiltration of carbon tetrachloride. Through numerical simulation, we have investigated the effective refractive index and dispersion according to the change of lattice parameters. The ultraflat, all-normal dispersion with $\Delta D = \pm 0.98$ ps/nm.km in the wavelength region of 1.394 µm - 1.734 µm is achieved. Four optical fibers with flat dispersion and small value at the pump wavelengths are proposed as low-power laser sources for studies on supercontinuum generation.

1. INTRODUCTION

Currently, supercontinuum generation (SCG) based on photonic crystal fibers (PCFs) is a hot topic attracting the attention of many research groups (Dudley et al., 2006; Agrawal, 2013). To produce good SCG, characterized by a broad spectrum and high coherence, a flat dispersion profile serves as one of the primary requirements. Fiber design for high nonlinearity and appropriate pump location selection are additional requirements to enhance SCG performance. Possessing many admirable properties such as design flexibility, broadband single-mode effect, good control over dispersion characteristics and good nonlinearity, PCFs can meet the demand for ultra-flat dispersion. The diversity in the structural design of PCFs such as cladding shape; number, size and shape of air holes; the shape and material of the core,... along with the selection of appropriate design parameters, contribute to achieving desired requirements for the dispersion and nonlinear characteristics in both numerical simulation and experimental fiber fabrication (Mahdiraji et al., 2014; Alam et al., 2021; Sharafali & Nithyanandan, 2020). Among them, ultra-flat dispersions are obtained for hollow-core PCFs infiltrated with nonlinear optical fluids, combined with appropriate modification of lattice parameters (Thi et al., 2023b; Thi et al., 2024; Van et al., 2022; Hoang et al., 2019). SCG uses nonlinear medium such as PCFs with many wide applications in the fields of optical communication, biomedicine, environment,... (Rao et al., 2021; Poudel & Kaminski, 2019). Furthermore, flat and broadband SCG sources with all-normal dispersion are suitable for the mid-infrared optical coherence tomography systems in the analysis of polymers, ceramics, and some biochemical elements (Paterova et al., 2017; Takamatsu et al., 2024).

Typically, the nonlinear effects occurring during the SCG process depend strongly on the dispersion profile when simulating the optical properties of PCFs. For PCFs with anomalous dispersion properties, soliton fission (SF), dispersive wave (DW) generation, and Raman soliton self-frequency shifting (RSSFS) are the main causes leading to the formation and evolution of SCG (Dudley et al., 2006). The resulting spectrum has a wide bandwidth but is often noisy. On the contrary, self-phase modulation (SPM) and optical wave breaking mechanism (OWB) (Heidt et al., 2011) largely contribute to creating a less noisy SCG spectrum. Thus, realizing high-quality SCG sources requires careful design of the PCF to achieve both all-normal and anomalous dispersion, high nonlinearity, and optimizing the initial laser pulse characteristics such as the pumping wavelength. By simulation and experiment, several publications have verified the possibility of broadband SCG

Corresponding author: Hoang Trong Duc;
E-mail address: hoangtrongduc@hueuni.edu.vn
DOI: https://doi.org/10.26459/jse.045.2026

using PCFs infiltrated with carbon tetrachloride (CCl_4) (Hoang et al., 2019; Dinh et al., 2018; Thi et al., 2022; Thi et al., 2023a; Le et al., 2021; Hoang et al., 2020). Compared with silica (SiO_2) ($n_2 = 15.3\times10^{-20}$ m^2/W), CCl_4 has a higher nonlinear coefficient ($n_2 = 1.53\times10^{-19}$ m^2/W) (Hoang et al., 2019; Ho & Alfano, 1979) about 10 times higher at a wavelength of 1.064 µm, which is the key factor that creates the refractive index difference between the cladding and core region, thereby increasing the ability to confine light into the core due to total reflection mechanism. Furthermore, carbon tetrachloride is less toxic than carbon disulfide, nitrobenzene, or toluene (Challenor, 2002). These interesting properties inspired us to choose it as a highly nonlinear optical fluid to fill the hollow core of PCFs.

In this paper, modifying the lattice parameters related to the size of the air pores and the distance between them in a CCl_4-filled PCF (CPCF) helps to optimize dispersion. We obtained an ultra-flat all-normal dispersion profile with a small value of ±0.98 ps/nm.km in the 0.34 µm wavelength region. The effective refractive index was also thoroughly investigated. Four PCFs with reasonable dispersion characteristics, including flatness, small value, and suitable zero dispersion wavelengths (ZDWs) are recommended as SCG sources for further studies.

2. NUMERICAL MODELING OF THE PCFS

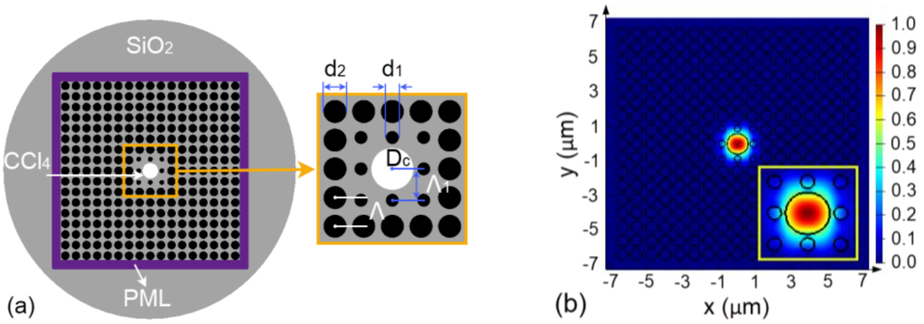

Figure 1. The image of hollow core PCF infiltrated with CCl_4 in two dimensions (a); The light is well confined in the core of the PCF with Λ = 0.8 µm, d_1/Λ = 0.45 at wavelength 1.55 µm (b).

The cladding region of the CPCFs has a square shape with eight layers of air holes separated by a distance Λ. In which the first layer of air holes near the core has diameter $d_1 = (0.3-0.8)\Lambda$, the second to eighth layers have diameter $d_2 = 0.8\Lambda$. The variation in air hole size contributes to achieving the desired optical properties. Although the work (Thi et al., 2023a) demonstrated improved dispersion and nonlinear properties of square lattice PCFs with CCl_4-infiltraed cores that are beneficial for SCG processes, the ultra-flat dispersion with small values in wide wavelength range has not yet been achieved. To further enhance the beneficial dispersion characteristics for broadband SCG, we set the difference in the distance of the air hole layers from the core, specifically the first air hole layer is at a distance of $\Lambda_1 = 1.093\Lambda$ from the center of the core while the distance between other air layers remains unchanged. The core is the biggest air hole, has a typical circular shape like a conventional fiber optics, with diameter $D_c = 2\Lambda - 1.2d_1$, filled with CCl_4 (figure 1a). Lumerical Mode Solution software is used to model this type of structure and solve the Maxwell wave equation with the full vector finite difference eigencoding method. The perfectly matched layers absorbing boundary condition are used to limit the simulation window. They are hundreds of thousands of rectangles with an area very small compared to the PCF cross-section so that the optical properties on each mesh do not change and the propagation coefficient is calculated with high precision. After running the simulation program, the light in the core region also indicates good mode field confinement (figure 1b).

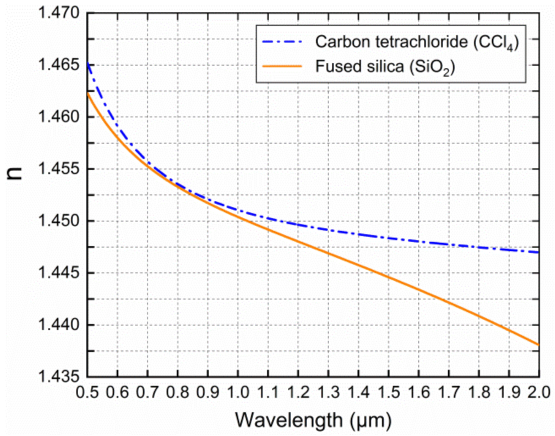

Figure 2. The real part plot of the refractive index of CCl_4 and SiO_2 depends on the wavelength extrapolated using the Sellmeier equation.

The refractive index of SiO_2 and CCl_4 materials varies with the change in wavelength and given by the Sellmeier's equation (Tan, 1998) and Cauchy's equation (Moutzouris et al., 2013):

$$n_{SiO_2}^2(\lambda) = 1 + \frac{0.6961663\lambda^2}{\lambda^2 - (0.0684043)^2} + \frac{0.4079426\lambda^2}{\lambda^2 - (0.1162414)^2} + \frac{0.8974794\lambda^2}{\lambda^2 - (9.896161)^2} \quad (1),$$

$$n_{CCl_4}^2 = 2.085608282 + 0.00053373\lambda^2 + 0.012201206\lambda^{-2} + 0.000056451\lambda^{-4} + 0.000048106\lambda^{-6} \quad (2),$$

where λ is the excitation wavelength in micrometers, $n(\lambda)$ is the wavelength-dependent linear refractive index of materials.

Figure 2 illustrates the dependence of the linear refractive index (n) of SiO_2 and CCl_4 extrapolated by (Tan, 1998; Moutzouris et al., 2013) on wavelength. The values of n decrease as the wavelength increases and these values of CCl_4 are always larger than SiO_2 in the studied wavelength range but the difference between the two values is not too large. This property is beneficial for the coupling between liquid core fibers and conventional SiO_2 fibers.

3. SIMULATION RESULTS AND ANALYSIS

3.1. The effective refraction index

Table 1. The value of real part of effective refraction index of CPCFs with various d_1/Λ and Λ at 1.55 μm wavelength

d_1/Λ	Λ = 0.8 μm	Λ = 0.9 μm	Λ = 1.5 μm	Λ = 2.0 μm
0.3	1.384	1.394	1.421	1.43
0.35	1.379	1.389	1.419	1.429
0.4	1.373	1.383	1.416	1.427
0.45	1.366	1.378	1.413	1.426
0.5	1.359	1.372	1.411	1.424
0.55	1.352	1.365	1.408	1.422
0.6	1.344	1.358	1.405	1.42
0.65		1.351	1.401	1.418
0.7		1.343	1.398	1.416
0.75			1.394	1.414
0.8			1.39	1.411

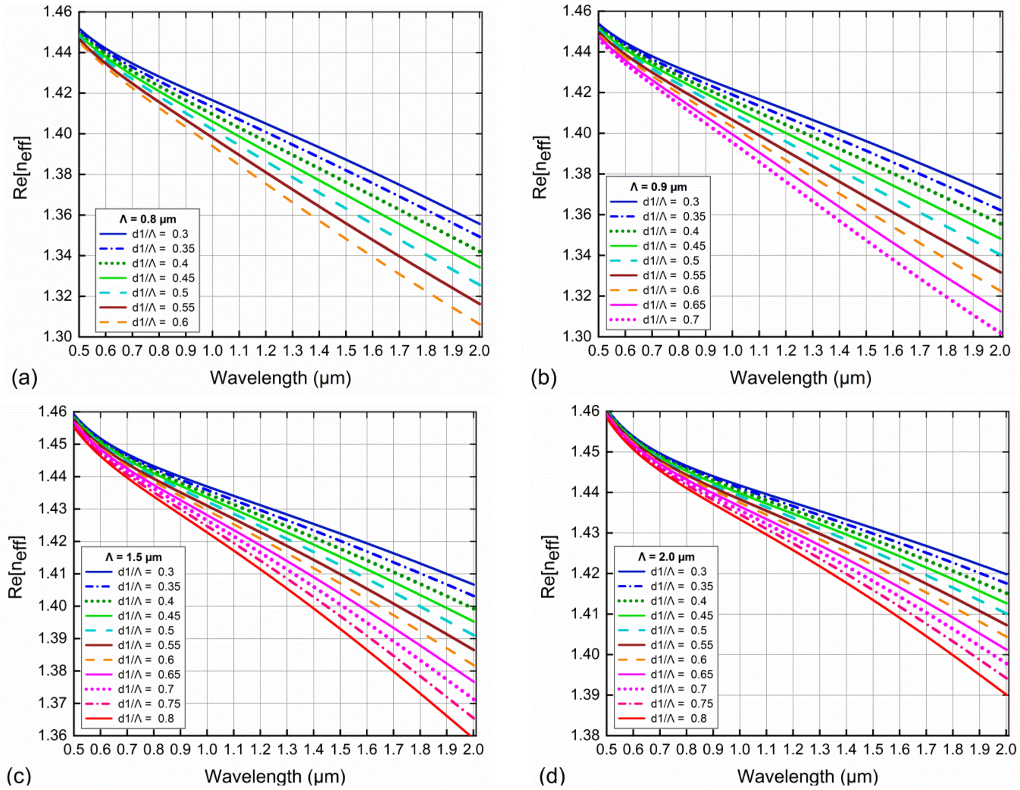

Figure 3. The real part of effective refraction index as a function of wavelength of CPCFs with various d_1/Λ and Λ = 0.8 μm (a), 0.9 μm (b), 1.5 μm (c), and 2.0 μm (d).

The refractive index of a medium's material changes when a strong input pulse propagates through a nonlinear medium, thereby altering the effective refractive index of fibers. The real part of the effective refractive index (Re[n_{eff}]) of CPCFs decreases with increasing wavelength, as displayed in figure 3. These values depend significantly on the lattice parameters d_1/Λ and Λ. When Λ is constant, Re[n_{eff}] decreases as d_1/Λ increases. The difference between the values becomes more pronounced in the wavelength region larger than 1.0 µm. Conversely, d_1/Λ is held constant, the values of Re[n_{eff}] increase with increasing Λ.

The values of the effective refractive index are calculated at a wavelength of 1.55 µm, and are presented in table 1. The maximum value of Re[n_{eff}], which is 1.43, corresponds to the case of d_1/Λ = 0.3 and Λ = 2.0 µm. PCFs with very small core sizes often exhibit poorer light interaction than large core PCFs, so the real part of the effective refractive index decreases as d_1/Λ increases (for each fixed Λ) (table 1).

3.2. The group velocity dispersion

The group velocity dispersion (D) is responsible for determining the range over which the spectral frequency components of the input pulse propagate in the PCF structure at different phase velocities. The D process is a function of wavelength depending on the efficiency indices of the propagation mode and can it be calculated as follows (Agrawal, 2013):

$$D = -\frac{\lambda}{c}\frac{\partial^2 \text{Re}[n_{eff}]}{\partial \lambda^2} \quad (3),$$

where c is the velocity of light in vacuum.

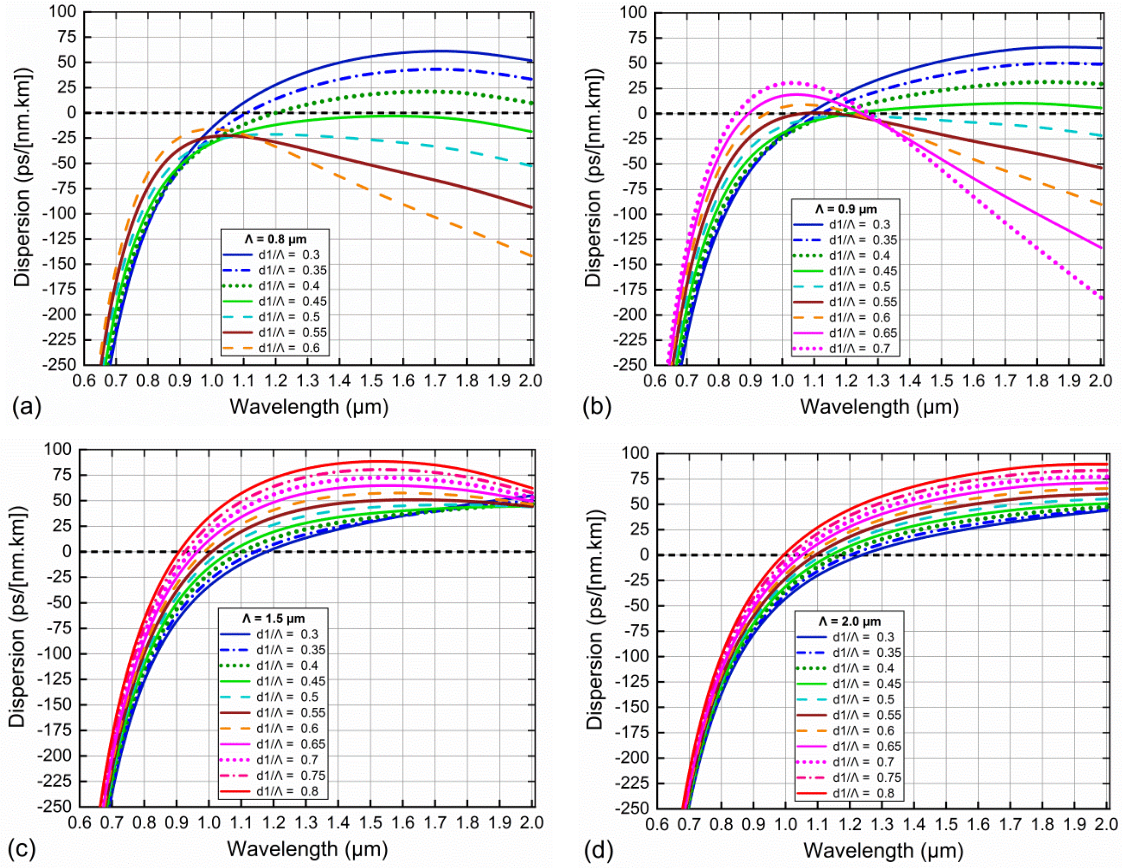

Figure 4. The dispersion of CPCFs with various d_1/Λ and Λ = 0.8 µm (a), 0.9 µm (b), 1.5 µm (c), and 2.0 µm (d).

As Λ and d_1/Λ varied, a significant change in the nature of the dispersion profile has been observed, with a larger shift in zero dispersion wavelengths (ZDWs) towards shorter wavelengths side for Λ = 1.5 and 2.0 µm compared to the dispersion curves for Λ = 0.8 and 0.9 µm, as illustrated in figure 4. In general, for small Λ, there is a diversity of dispersion profile including all-normal and anomalous dispersion characteristics with one or two ZDWs. When Λ = 0.8 µm, the dispersion curves are anomalous to a ZDW with d_1/Λ less than 0.45. With a gradually increasing d_1/Λ, the curves lie below the zero dispersion line, indicating all-normal dispersion. An ultra-flat dispersion configuration with fluctuations of ±0.98 ps/nm.km has been achieved in the wavelength range from 1.394 µm to 1.734 µm with structural parameters Λ = 0.8 µm and d_1/Λ = 0.45. For

Λ = 0.9 μm, an all-normal dispersion profile is observed when d_1/Λ = 0.5, while the remaining PCFs exhibit anomalous dispersion profiles with one or two ZDWs. With further increasing in Λ, the dispersion curves increasingly shift above the zero dispersion line as d_1/Λ increases, they are all anomalous dispersion with one ZDW. Therefore, the majority of flat dispersion curves with low values are observed for the case of Λ = 0.8 and 0.9 μm. These are interesting suggestions for appropriate dispersion profile for studying the SCG. The results of ultra-flat dispersion with PCFs filled with CCl_4 are similar to some previous papers using liquids such as toluene (Thi et al., 2023b), tetrachloroethylene (Van et al., 2022), ethanol (Le et al., 2018), benzene (Duc & Thuy, 2023).

ZDW values play a crucial role in determining the location of injecting fibers during the SCG process. Typically, the pump wavelengths are determined to minimize their dispersion values and to be as low and as close to 1.55 μm (commercial laser source) as possible, which directly affects the broadening of the SCG spectrum. The ZDW values of CPCF are verified in table 2.

Table 2. ZDWs values of CPCFs

	Λ = 0.8 μm	Λ = 0.9 μm		Λ = 1.5 μm	Λ = 2.0 μm
d_1/Λ	ZDW_1	ZDW_1	ZDW_2	ZDW_1	ZDW_1
0.3	1.055	1.085		1.177	1.234
0.35	1.108	1.12		1.142	1.201
0.4	1.199	1.158		1.101	1.167
0.45	D < 0	1.212		1.067	1.14
0.5	D < 0	D < 0		1.034	1.115
0.55	D < 0	1.057	1.168	1.008	1.091
0.6	D < 0	0.946	1.226	0.983	1.071
0.65		0.891	1.252	0.963	1.051
0.7		0.855	1.274	0.943	1.03
0.75				0.925	1.012
0.8				0.907	0.993

To investigate the characteristics of the SCG spectrum, researchers often select the pump wavelength in the normal ($D < 0$) or anomalous ($D > 0$) dispersion region of the dispersion curve. The ZDWs divide the dispersion curve into two or more different dispersion regions. Depending on the specific objectives of SCG with different applications, PCFs with appropriate dispersion profile are recommended. When a high-intensity pulse is excited at a specific pump wavelength propagating in a nonlinear medium, it will strongly interact with the medium and cause some typical nonlinear effects (SF, DW, RSSFS, SPM, and OWB) as introduced in section 1. These nonlinear effects are responsible for the diverse characteristics of the SCG spectrum, including the width, flatness or ultra-flatness, coherence, noise. Based on the aforementioned results on dispersion properties, we propose four CPCFs (named F_1, F_2, F_3, F_4 respectively) with flat dispersion, low values, and recommend suitable pump wavelengths for further research on SCG, as depicted in figure 5.

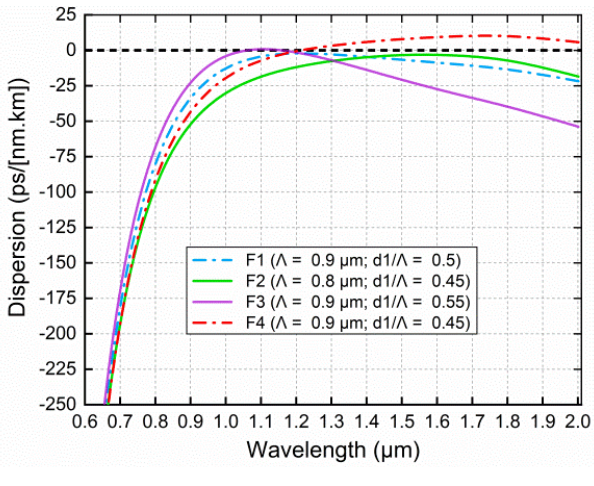

Figure 5. The dispersion properties of the four proposed CPCFs.

Fibers F_1 (Λ = 0.9 μm, d_1/Λ = 0.5) and F_2 (Λ = 0.8 μm, d_1/Λ = 0.45) both exhibit all-normal dispersion, in which F_2 has ultra-flat dispersion with the flatness in the range of 0.34 μm and ΔD = ±0.98 ps/nm.km. These two fibers are expected to emit broadband SCG spectrum, low noise, and high coherence, primarily influenced by SPM and OWB effects. When using these two fibers for the SCG process, we can compare to see how the F_2 fiber with ultra-flat dispersion, low values in a wide wavelength range affects the spectrum. Since fiber F_1 has the local maximum of the dispersion curve at wavelengths shorter than 1.55 µm, we choose a pump wavelength of 1.25 µm, whereas a pump wavelength of 1.55 µm is recommended for fiber F_2. The two fibers F_3 (Λ = 0.9 µm, d_1/Λ = 0.55) and F_4 (Λ = 0.9 µm, d_1/Λ = 0.45) both exhibit anomalous dispersion, with low values near zero dispersion. F_3 has a typical parabolic dispersion profile with two ZDWs very close to each other (ZDW1 = 1.057 µm and ZDW2 = 1.168 µm), with the pump wavelength of 1.064 µm located in the anomalous dispersion region between the two ZDWs. These fibers often generate a broad SCG spectrum with interesting properties due to soliton suppression. With flat anomalous dispersion with one ZDW, low value at the pump wavelength of 1.25 µm, the F_4 fiber enables a very broad but noisy spectrum with nonlinear mechanisms related to soliton dynamics. The structural parameters and dispersion values at the pump wavelengths of the four proposed CPCFs are computed in table 3.

Table 3. The characteristic quantities at the pump wavelengths of the four proposed CPCFs

#	D_c	Λ	d_1/Λ	Pump wavelength	Re[n_{eff}]	D
	(µm)	(µm)		(µm)		(ps/(nm.km))
F_1	1.26	0.9	0.50	1.25	1.392	−2.168
F_2	1.17	0.8	0.45	1.55	1.366	−2.951
F_3	1.21	0.9	0.55	1.064	1.402	0.227
F_4	1.31	0.9	0.45	1.25	1.397	1.66

4. CONCLUSION

We used LMS to model 38 PCFs structures with CCl4 infiltrated cores and investigated in detail their optical properties, including effective refractive index and dispersion. The role of lattice defects, such as differences in air hole size and distance between them, is emphasized in improving the dispersion of PCFs, which is essential for SCG research. Interestingly, we have achieved ultra-flat dispersion with flatness spanning a wavelength range as broad as 0.34 µm, with small fluctuations of ±0.98 ps/nm.km. Four structures with optimal dispersion are proposed for further studies on the SCG process. The low dispersion values, on the order of a few ps/nm.km, and the well-recommended pump wavelengths are ideal for studying SCG with low input peak power. These proposed CCl_4 core fibers can be an effective source of SCG, replacing the previous traditional glass fibers.

REFERENCES

Agrawal, G. P. (2013). *Nonlinear fiber optics* (5th ed.). Academic Press, Elsevier. https://doi.org/10.1016/C2011-0-00045-5

Alam, M. Z., Tahmid, M. I., Mouna, S. T., Islam, M. A., & Alam, M. S. (2021). Design of a novel star type photonic crystal fiber for mid-infrared supercontinuum generation. *Optics Communications, 500*, 127322. https://doi.org/10.1016/j.optcom.2021.127322

Challenor, J. (2002). *Toxicology of solvents*. Rapra Technology Ltd.

Dinh, Q. H., Pniewski, J., Van, H. L., Ramaniuk, A., Long, V. C., Borzycki, K., Xuan, K. D., Klimczak, M., & Buczyński, R. (2018). Optimization of optical properties of photonic crystal fibers infiltrated with carbon tetrachloride for supercontinuum generation with subnanojoule femtosecond pulses. *Applied Optics, 57*, 3738–3746. https://doi.org/10.1364/AO.57.003738

Duc, H. T., & Thuy, N. T. (2023). An ultra-flattened chromatic dispersion in circular C6H6-infiltrated photonic crystal fibers. *Science & Technology Development Journal, 26*, 1–13. https://doi.org/10.32508/stdj.v26i2.4074

Dudley, J. M., Genty, G., & Coen, S. (2006). Supercontinuum generation in photonic crystal fiber. *Reviews of Modern Physics, 78*, 1135–1184. https://doi.org/10.1103/RevModPhys.78.1135

Heidt, A. M., Hartung, A., Bosman, G. W., Krok, P., Rohwer, E. G., Schwoerer, H., & Bartelt, H. (2011). Coherent octave spanning near-infrared and visible supercontinuum generation in all-normal dispersion photonic crystal fibers. *Optics Express, 19*, 3775–3787. https://doi.org/10.1364/OE.19.003775

Ho, P. P., & Alfano, R. R. (1979). Optical Kerr effect in liquids. *Physical Review A, 20*, 2170–2187. https://doi.org/10.1103/PhysRevA.20.2170

Hoang, V. T., Kasztelanic, R., Filipkowski, A., Stępniewski, G., Pysz, D., Klimczak, M., Ertman, S., Long, V. C., Woliński, T. R., Trippenbach, M., Xuan, K. D., Śmietana, M., & Buczyński, R. (2019). Supercontinuum generation in an all-normal dispersion large core photonic crystal fiber infiltrated with carbon tetrachloride. *Optical Materials Express, 9*, 2264–2278. https://doi.org/10.1364/OME.9.002264

Hoang, V. T., Kasztelanic, R., Stępniewski, G., Xuan, K. D., Long, V. C., Trippenbach, M., Klimczak, M., Buczyński, R., & Pniewski, J. (2020). Femtosecond supercontinuum generation around 1560 nm in hollow-core photonic crystal fibers filled with carbon tetrachloride. *Applied Optics, 59*, 3720–3725. https://doi.org/10.1364/AO.385003

Le, H. V., Cao, V. L., Nguyen, H. T., Nguyen, A. M., Buczyński, R., & Kasztelanic, R. (2018). Application of ethanol infiltration for ultra-flattened normal dispersion in fused silica photonic crystal fibers. *Laser Physics, 28*, 115106. https://doi.org/10.1088/1555-6611/aad93a

Le, H. V., Hoang, V. T., Stępniewski, G., Canh, T. L., Minh, N. V. T., Kasztelanic, R., Klimczak, M., Pniewski, J., Dinh, K. X., Heidt, A. M., & Buczyński, R. (2021). Low pump power coherent supercontinuum generation in heavy metal oxide solid-core photonic crystal fibers infiltrated with carbon tetrachloride covering 930–2500 nm. *Optics Express, 29*, 39586–39600. https://doi.org/10.1364/OE.443666

Mahdiraji, G. A., Chow, D. M., Sandoghchi, S. R., Amirkhan, F., Dermosesian, E., Yeo, K. S., Kakaei, Z., Ghomeishi, M., Poh, S. Y., Gang, S. Y., & Adikan, F. R. M. (2014). Challenges and solutions in fabrication of silica-based photonic crystal fibers: An experimental study. *Fiber and Integrated Optics, 33*, 85–104. https://doi.org/10.1080/01468030.2013.879680

Moutzouris, K., Papamichael, M., Betsis, S. C., Stavrakas, I., Hloupis, G., & Triantis, D. (2013). Refractive, dispersive and thermo-optic properties of twelve organic solvents in the visible and near-infrared. *Applied Physics B, 116*, 617–622. https://doi.org/10.1007/s00340-013-5744-3

Paterova, A. V., Yang, H., An, C., Kalashnikov, D. A., & Krivitsky, L. A. (2017). Tunable optical coherence tomography in the infrared range using visible photons. *Quantum Science and Technology, 3*, 025008. https://doi.org/10.1088/2058-9565/aab567

Poudel, C., & Kaminski, C. F. (2019). Supercontinuum radiation in fluorescence microscopy and biomedical imaging applications. *Journal of the Optical Society of America B, 36*, A139–A153. https://doi.org/10.1364/JOSAB.36.00A139

Rao, D. S. S., Jensen, M., Grüner-Nielsen, L., Olsen, J. T., Heiduschka, P., Kemper, B., Schnekenburger, J., Glud, M., Mogensen, M., Israelsen, N. M., & Bang, O. (2021). Shot-noise limited, supercontinuum-based optical coherence tomography. *Light: Science & Applications, 10*, 133. https://doi.org/10.1038/s41377-021-00574-x

Sharafali, A., & Nithyanandan, K. (2020). A theoretical study on the supercontinuum generation in a novel suspended liquid core photonic crystal fiber. *Applied Physics B, 126*, 55. https://doi.org/10.1007/s00340-020-7403-9

Takamatsu, T., Fukushima, R., Sato, K., Umezawa, M., Yokota, H., Soga, K., Hernandez-Guedes, A., Callico, G. M., & Takemura, H. (2024). Development of a visible to 1600 nm hyperspectral imaging rigid-scope system using supercontinuum light and an acousto-optic tunable filter. *Optics Express, 32*, 16090–16102. https://doi.org/10.1364/OE.515747

Tan, C. Z. (1998). Determination of refractive index of silica glass for infrared wavelengths by IR spectroscopy. *Journal of Non-Crystalline Solids, 223*, 158–163. https://doi.org/10.1016/S0022-3093(97)00438-9

Thi, T. N., Trong, D. H., & Van, L. C. (2023a). Comparison of supercontinuum spectral widths in CCl4-core PCF with square and circular lattices in the claddings. *Laser Physics, 33*, 055102. https://doi.org/10.1088/1555-6611/acc240

Thi, T. N., Trong, D. H., & Van, L. C. (2023b). Supercontinuum generation in ultra-flattened near-zero dispersion PCF with C7H8 infiltration. *Optical and Quantum Electronics, 55*, 93. https://doi.org/10.1007/s11082-022-04351-x

Thi, T. N., Trong, D. H., & Van, L. C. (2024). Optimization of dispersions in benzene-core square photonic crystal fibers for mid-infrared supercontinuum generation with very low peak power. *Optik, 304*, 171754. https://doi.org/10.1016/j.ijleo.2024.171754

Thi, T. N., Trong, D. H., Tran, B. T. L., & Van, L. C. (2023). Flat-top and broadband supercontinuum generation in CCl4-filled circular photonic crystal fiber. *Journal of Nonlinear Optical Physics & Materials*. https://doi.org/10.1142/S021886352350042X

Van, L. C., Le, H. V., Nguyen, N. D., Minh, N. V. T., Dinh, Q. H., Hoang, V. T., Thi, T. N., & Van, B. C. (2022). Modelling of lead-bismuth gallate glass ultra-flatted normal dispersion photonic crystal fiber infiltrated with tetrachloroethylene for high coherence mid-infrared supercontinuum generation. *Laser Physics, 32*, 055102. https://doi.org/10.1088/1555-6611/ac599b

Mô phỏng số đặc tính tán sắc trong sợi tinh thể quang tử mạng vuông thẩm thấu CCl_4

Siu Lol[1], Nguyễn Thị Thủy[2], Hoàng Trọng Đức[2]

[1]*Trường Trung học phổ thông Nguyễn Du số 2, xã Uar, tỉnh Gia Lai*

[2]*Trường Đại học Sư phạm, Đại học Huế*

THÔNG TIN BÀI BÁO

Quá trình xử lý:
Ngày nhận bài: 27/4/2024
Ngày nhận bản chỉnh sửa: 21/6/2024
Ngày nhận đăng: 24/6/2024
Ngày xuất bản: 20/04/2026

Từ khóa:
Sợi tinh thể quang tử;
Carbon tetrachloride;
Tán sắc hoàn toàn bình thường siêu phẳng;
Phát siêu liên tục.

Tác giả liên hệ:
Hoàng Trọng Đức
Địa chỉ e-mail:
hoangtrongduc@hueuni.edu.vn

TÓM TẮT

Các khuyết tật mạng tinh thể, bao gồm sự khác biệt về kích thước lỗ khí và khoảng cách giữa các lỗ khí, đã góp phần đáng kể vào việc tối ưu đặc tính tán sắc của sợi tinh thể quang tử mạng vuông được thẩm thấu carbon tetrachloride. Thông qua mô phỏng số, chúng tôi đã khảo sát sự phụ thuộc của chiết suất hiệu dụng và tán sắc theo sự thay đổi của các tham số cấu trúc. Kết quả cho thấy có thể đạt được đặc tính tán sắc hoàn toàn bình thường siêu phẳng với dao động $\Delta D = \pm 0{,}98$ ps/nm·km trong dải bước sóng từ 1,394 µm đến 1,734 µm. Bốn sợi quang có cấu hình tán sắc phẳng, giá trị nhỏ tại các bước sóng bơm đã được đề xuất như những nguồn laser công suất thấp cho các nghiên cứu về tạo phổ siêu liên tục.